DALTON
FULL PAPER

Trinuclear $Cu^{II}M^{II}Cu^{II}$ complexes of an oxamide/dioxime ligand and extension to a bimetallic magnetic compound

Nobuo Fukita,[a] Masaaki Ohba,[a] Takuya Shiga,[a] Hisashi Ōkawa *[a] and Yoshitami Ajiro[b]

[a] *Department of Chemistry, Faculty of Sciences, Kyushu University, Hakozaki 6-10-1, Higashiku, Fukuoka 812-8581, Japan*
[b] *Department of Physics, Faculty of Sciences, Kyushu University, Hakozaki 6-10-1, Higashiku, Fukuoka 812-8581, Japan*

Received 14th August 2000, Accepted 10th October 2000
First published as an Advance Article on the web 7th December 2000

N,*N*′-Bis[2-(hydroxyiminomethyl)phenyl]oxamide (H_4L) provided trinuclear $Cu^{II}M^{II}Cu^{II}$ complexes $[M\{Cu(HL)(DMF)\}_2(DMF)_2]$ (M^{II} = Mn **1**, Co **2**, Ni **3** or Zn **4**). The crystal structures of **1**–**4** have been determined by X-ray crystallography. They are isomorphous and have an oxamidate-bridged trinuclear $Cu^{II}M^{II}Cu^{II}$ structure. The Cu^{II} resides in a pseudo-macrocyclic framework of $(HL)^{3-}$ comprised of an oxamidate and a hydrogen-bonded dioximate (=N–O · · · H · · · O–N=) groups to form a square-pyramidal structure {Cu(HL)(DMF)} together with a DMF molecule. Two {Cu(HL)(DMF)} entities co-ordinate to a Mn^{II} through the oxamidate oxygens to afford a *cis* octahedral environment about the metal together with two DMF oxygens. The $Cu^{II} \cdots M^{II}$ intermetallic distance separated by the oxamidate bridge is 5.33–5.49 Å. In the case of **1** and **3** a significant antiferromagnetic interaction operates between the adjacent Cu^{II} and M^{II}. The reaction of **1** with Mn^{II} in acetonitrile in the presence of KOH and 18-crown-6 formed $Mn\{Cu(L)\}(H_2O)_4$ that has a polymeric structure extended by the dioximate–Mn^{II}–dioximate linkage. It is a weak ferromagnet (T_C = 5.5 K) exhibiting a weak antiferromagnetic interaction between the ferrimagnetic chains.

Introduction

The design of molecular-based magnetic materials is a current subject of many studies.[1–4] The use of paramagnetic metal complexes as the constituents has great advantages over organic radical constituents because electron spin can be reserved to each metal center, 1-D to 3-D network structures can be constructed based on versatile stereochemistries of metal complexes, and the magnetic nature of complex-based magnets can be tuned by choice of metal ion and bridging group.[5,6] For constructing complex-based network structures, 'complex bridges' are generally used that have two or more sites capable of acting as bridges to outer metal ions.

The bridging function of oxamidate groups is well known.[7–12] One of the present authors used *N*,*N*-bis(3-aminopropyl)-oxamidatocopper(II) as a 'complex ligand' to obtain triangular tetranuclear $M^{II}Cu^{II}_3$ complexes with the M^{II} at the center and Cu^{II} at the corners of the triangle.[7] These and related complexes[9] showed a significant antiferromagnetic interaction between the adjacent Cu^{II} and M^{II} through the oxamidate bridge in *cis* arrangement. Oxamidate bridges in *trans* arrangement are similarly good magnetic mediators and have been used for providing bimetallic magnetic materials.[9–12] The oximate group (=N–O$^-$) is another magnetic mediator between metal ions.[13–22] In a trinuclear copper(II) complex derived from bis(dimethylglyoximato)cuprate(II) complete spin coupling occurs at room temperature through the dioximate bridge in *cis* arrangement.[18] Significant antiferromagnetic interaction between dissimilar ions of Cu^{II} and M^{II} through a dioximate bridge has been reported.[19,22]

In the context mentioned above, *N*,*N*′-bis[2-(hydroxyiminomethyl)phenyl]oxamide (Fig. 1), abbreviated as H_4L, has been prepared in this work. Its mononuclear copper(II) complex $[Cu(HL)]^-$ is expected to act as a 'complex bridge' with its oxamidate and dioximate termini. Trinuclear $Cu^{II}M^{II}Cu^{II}$ complexes $[M\{Cu(HL)(DMF)\}_2(DMF)_2]$ (M^{II} = Mn **1**, Co **2**, Ni **3** or Zn **4**) have been prepared and characterized by X-ray crystallography and cryomagnetic studies. An extension of **1** into a polymeric compound $Mn\{Cu(L)\}(H_2O)_4$ exhibiting a magnetic phase transition at T_c = 5.5 K is reported.

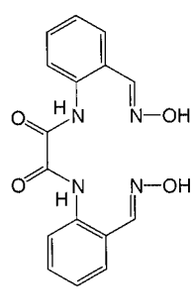

Fig. 1 Chemical structure of H_4L.

Experimental

Physical measurements

Elemental analyses of C, H and N were obtained at the Service Center of Elemental Analysis of Kyushu University, metal analyses using a Shimadzu A-A 680 Atomic Absorption/Flame Emission Spectrophotometer. Infrared spectra were measured on KBr disks with a Perkin-Elmer Spectrum BX FT-IR system, Reflectance spectra on powdered samples with a Shimadzu UV-3100PC spectrophotometer using an integrating sphere attachment. Magnetic susceptibilities were measured using a Quantum Design MPMS 5XL or MPMS2 SQUID susceptometer in the temperature range 2–300 K. Calibrations were made with the standard Pd. Data were corrected for magnetization of the sample holder and capsule used. Diamagnetic corrections were made using Pascal's constants.[23] Magnetization studies were carried out with the same apparatus.

 DOI: 10.1039/b006613n

Preparations

N,*N*′-Bis(2-formylphenyl)oxamide was prepared by the literature method.[24] All chemicals were of reagent grade used as purchased.

***N*,*N*′-Bis[2-(hydroxyiminomethyl)phenyl]oxamide (H_4L).** *N*,*N*′-Bis(2-formylphenyl)oxamide (2.96 g, 10 mmol) and hydroxylammonium chloride (1.39 g, 20 mmol) were added to ethanol–water (1 : 1 in volume, 500 ml) and the mixture was refluxed for 3 hours. *N*,*N*′-Bis(2-formylphenyl)oxamide itself was insoluble in the mixed solvent but gradually dissolved to form a clear yellow solution. It was evaporated to dryness, and the resulting yellow residue treated with a saturated $NaHCO_3$ solution (300 ml) and washed with water. Crystallization from hot ethanol gave pale yellow needles melting at 284 °C. The yield was 2.31 g (71%). Calc. for $C_8H_7N_2O_2$: C, 58.89; H, 4.32; N, 17.17%. Found: C, 58.91; H, 4.37; N, 17.12%. ^{1}H NMR [d_6-DMF]: δ 7.32 (t(2H), ring proton), 7.51(t(2H), ring proton), 7.61(d(4H), ring proton), 8.45(s(2H), ArCH=N), 8.68(d(2H), ArNHC) and 12.46(s(2H), NOH). Selected FT-IR using KBr: $\tilde{\nu}$/cm^{-1} 3540, 3272, 1691, 1578, 1315, 1293, 1007 and 750.

[Mn{Cu(HL)(DMF)}$_2$(DMF)$_2$] 1. H_4L (163 mg, 0.5 mmol) was dissolved in DMF (*N*,*N*-dimethylformamide) (50 ml) and an aqueous solution of NaOH (80 mg, 2 mmol) added. A DMF solution of copper(II) acetate monohydrate (100 mg, 0.5 mmol) was added dropwise and the mixture stirred for 30 minutes. A DMF solution of manganese(II) acetate tetrahydrate (61 mg, 0.25 mmol) was then added, and the mixture diffused with diethyl ether to form dark green crystals. The yield was 182 mg (65%). Calc. for $C_{44}H_{50}Cu_2MnN_{12}O_{12}$: C, 47.14; H, 4.50; Cu, 11.34; Mn, 4.9; N, 14.99%. Found: C, 47.06; H, 4.63; Cu, 10.90; Mn, 4.6; N, 14.62%. Selected FT-IR using KBr: $\tilde{\nu}$/cm^{-1} 1664, 1639, 1603, 1569, 1558, 1337, 920 and 756. Visible spectrum on powdered sample: λ/nm 525 and 600.

[Co{Cu(HL)(DMF)}$_2$(DMF)$_2$] 2. This complex was obtained as dark green crystals similarly to **1**, using cobalt(II) acetate tetrahydrate. The yield was 196 mg (70%). Calc. for $C_{44}H_{50}CoCu_2N_{12}O_{12}$: C, 46.98; H, 4.48; Co, 5.2; Cu, 11.30; N, 14.94%. Found: C, 46.71; H, 4.65; Co, 5.0; Cu, 10.83; N, 14.62%. Selected FT-IR using KBr: $\tilde{\nu}$/cm^{-1} 2928, 1664, 1640, 1557, 1336, 920 and 756. Visible spectrum on powdered sample: λ/nm 515 and 600.

[Ni{Cu(HL)(DMF)}$_2$(DMF)$_2$] 3. This complex was obtained as dark green crystals similarly to **1**, using nickel(II) acetate tetrahydrate. The yield was 168 mg (60%). Calc. for $C_{44}H_{50}Cu_2N_{12}NiO_{12}$: C, 46.99; H, 4.48; Cu, 11.30; Ni, 5.2; N, 14.94%. Found: C, 47.07; H, 4.71; Cu, 11.03; Ni, 5.5; N, 14.41%. Selected FT-IR using KBr: $\tilde{\nu}$/cm^{-1} 2928, 1663, 1636, 1555, 1341, 920 and 756. Visible spectrum on powdered sample: λ/nm 515, 600 and 965.

[Zn{Cu(HL)(DMF)}$_2$(DMF)$_2$] 4. This complex was obtained as dark green crystals similarly to **1**, using zinc(II) acetate tetrahydrate. The yield was 170 mg (60%). Calc. for $C_{44}H_{50}Cu_2N_{12}O_{12}Zn$: C, 46.71; H, 4.45; Cu, 11.23; N, 14.86; Zn, 5.8%. Found: C, 46.80; H, 4.45; Cu, 11.43; N, 14.86; Zn, 6.3%. Selected FT-IR using KBr: $\tilde{\nu}$/cm^{-1} 2928, 1663, 1637, 1604, 1557, 1339, 920 and 756. Visible spectrum on powdered sample: λ/nm 515 and 600.

Mn{Cu(L)}(H$_2$O)$_4$ 5. To a solution of complex **1** (224 mg, 0.2 mmol) in CH_3CN–water (1 : 1 in volume, 50 ml) were added KOH (22 mg, 0.4 mmol) and 18-crown-6 (105 mg, 0.4 mmol). To the resulting solution was added manganese(II) perchlorate hexahydrate (72 mg, 0.2 mmol) and the mixture stirred to give a brown crystalline powder. It was collected, washed with diethyl ether and dried *in vacuo* over P_2O_5. The yield was 82 mg (80%). Calc. for $C_{16}H_{18}CuMnN_4O_8$: C, 37.48; H, 3.54; Cu, 12.39; Mn, 10.71; N, 10.93%. Found: C, 37.48; H, 3.89; Cu, 12.86; Mn, 10.93; N, 10.42%. Selected FT-IR using KBr: $\tilde{\nu}$/cm^{-1} 1615, 1562, 1333, 916 and 754. Visible spectrum on powdered sample: λ/nm 500 and 590.

Crystal structural analyses

Each single crystal of complexes **1**–**4** was mounted on a glass fiber and coated with epoxy resin. Intensities and lattice parameters were obtained on a Rigaku AFC-5S automated four-circle diffractometer with graphite-monochromated Mo-Kα radiation (λ = 0.71069 Å) for **2** and a Rigaku AFC-7R automated four-circle diffractometer with graphite-monochromated MoKα radiation (λ = 0.71069 Å) and 12 kW rotating anode generator for **1**, **3** and **4**. Cell constants and the orientation matrix for the data collection were obtained from 25 reflections and the ω–2θ scan mode was used for the intensity collections at 23 ± 1 °C. Pertinent crystallographic parameters are summarized in Table 1.

Three standard reflections were monitored every 150 measurements. A linear correction factor was applied to the data to account for decay. Intensity data were corrected for Lorentz and polarization effects.

The structures were solved by the direct method and expanded using Fourier techniques. Non-hydrogen atoms were refined anisotropically. Hydrogen atoms were included in the structure analysis but not refined. Computation were carried out on an IRIS O_2 computer using TEXSAN.[25]

CCDC reference number 186/2228.

See http://www.rsc.org/suppdata/dt/b0/b006613n/ for crystallographic files in .cif format.

Results and discussion

Synthesis and general properties

In spite of many efforts, all attempts to isolate a mononuclear copper(II) precursor complex of H_4L were in vain. Thus, this was prepared in solution and treated with a second metal(II) ion to provide the trinuclear complexes [M{Cu(HL)(DMF)}$_2$(DMF)$_2$] **1**–**4**. They show complicated IR bands in the region 2300–3000 cm^{-1}, which are characteristic of the hydrogen-bonded –O–H···O– linkage of the dioximate group.[26,27] The ν(C=O) band of the oxamidate group is seen around 1635–1640 cm^{-1}, which is low relative to that of H_4L (1691 cm^{-1}). This is in accord with the bridging function of the group as discussed below. An IR band around 1663 cm^{-1} is assigned to the ν(C=O) mode of the co-ordinating DMF.

The reflectance spectrum of compound **1** ($Cu^{II}Mn^{II}Cu^{II}$) shows two visible bands at 525 and 600 nm which are attributed to the d–d components of Cu^{II}: Mn^{II} in a high-spin state has no spin-allowed d–d band. Compound **4** ($Cu^{II}Zn^{II}Cu^{II}$) also shows two visible bands at 515 and 600 nm. A similar visible spectrum was obtained for **2** ($Cu^{II}Co^{II}Cu^{II}$). It is considered that the d–d bands of octahedral Co^{II} are weak and concealed by those of Cu^{II}. In the case of **3** ($Cu^{II}Ni^{II}Cu^{II}$) an additional band is observed at 965 nm that is assigned to a d–d component of Ni^{II}.

Crystal structures

Complexes **1**–**4** are isostructural. An ORTEP[28] drawing of **1** with the atom numbering scheme is given in Fig. 2. Selected bond distances and angles for **1**–**4** are summarized in Table 2.

The asymmetric unit consists of half of the [Mn{Cu(HL)(DMF)}$_2$(DMF)$_2$]: the Mn exists on the mirror plane. The Cu resides in the N_4 cavity of the ligand with two oxamidate nitrogens and two oxime nitrogens. The geometry about the Cu is square pyramidal with N(1), N(2), N(3) and N(4) of $(HL)^{3-}$

Table 1 Crystal parameters for complexes **1**–**4**

	1	**2**	**3**	**4**
Formula	$C_{44}H_{50}Cu_2MnN_{12}O_{12}$	$C_{44}H_{50}CoCu_2N_{12}O_{12}$	$C_{44}H_{50}Cu_2N_{12}NiO_{12}$	$C_{44}H_{50}Cu_2N_{12}O_{12}Zn$
Formula weight	1120.98	1124.98	1124.74	1131.42
Crystal system	Monoclinic	Monoclinic	Monoclinic	Monoclinic
Space group	*C*2/*c* (no. 15)	*C*2/*c* (no. 15)	*C*2/*c* (no. 15)	*C*2/*c* (no. 15)
a/Å	24.904(4)	24.903(5)	24.86(1)	24.910(4)
b/Å	10.229(2)	10.222(4)	10.279(3)	10.245(3)
c/Å	19.581(2)	19.569(6)	19.373(5)	19.459(3)
β/°	103.93(1)	103.87(2)	104.86(3)	104.72(1)
V/Å^3	4841(1)	4836(2)	4784(2)	4802(1)
Z	4	4	4	4
μ(Mo-Kα)/cm^{-1}	12.12	12.85	13.45	14.48
No. observations ($I > 3.00\sigma(I)$)	2996	2831	1537	2082
R	0.043	0.049	0.063	0.049
Rw	0.051	0.058	0.068	0.050

Table 2 Selected bond distances (Å) and angles (°) for complexes **1**–**4**

	M = Mn (**1**)	Co (**2**)	Ni (**3**)	Zn (**4**)
Cu–N(1)	1.991(4)	1.988(4)	1.99(1)	1.991(6)
Cu–N(2)	1.998(4)	1.999(4)	1.99(1)	2.009(6)
Cu–N(3)	2.014(4)	2.007(5)	2.01(1)	2.012(7)
Cu–N(4)	1.976(4)	1.989(5)	1.99(1)	1.987(6)
Cu–O(5)	2.378(4)	2.375(4)	2.38(1)	2.376(6)
M–O(1)	2.174(4)	2.173(4)	2.052(9)	2.103(5)
M–O(2)	2.167(3)	2.163(3)	2.022(9)	2.064(5)
M–O(6)	2.159(4)	2.159(5)	2.04(1)	2.089(6)
N(1)–Cu–N(2)	84.2(1)	83.8(2)	84.0(5)	84.0(2)
N(1)–Cu–N(3)	89.0(2)	89.0(2)	89.5(5)	89.2(3)
N(1)–Cu–N(4)	172.7(1)	172.7(2)	171.0(5)	171.7(3)
N(2)–Cu–N(3)	164.1(1)	164.1(2)	164.6(4)	164.7(3)
N(2)–Cu–N(4)	90.7(1)	91.1(2)	90.4(5)	90.3(3)
N(3)–Cu–N(4)	94.6(2)	94.7(2)	94.1(5)	94.9(3)
O(1)–M–O(1)*	93.6(2)	93.5(2)	94.4(5)	94.5(3)
O(1)–M–O(2)	74.3(1)	74.5(1)	79.7(3)	78.1(2)
O(1)–M–O(2)*	97.7(1)	97.7(1)	96.0(3)	95.8(2)
O(1)–M–O(6)	91.3(1)	91.2(2)	90.8(4)	90.7(2)
O(1)–M–O(6)*	163.8(1)	163.8(2)	170.8(4)	168.4(2)
O(2)–M–O(2)*	168.6(2)	168.8(2)	173.6(6)	171.2(3)
O(2)–M–O(6)	98.5(1)	98.4(2)	92.3(4)	95.4(2)
O(2)–M–O(6)*	89.7(1)	89.6(2)	92.4(4)	91.1(2)
O(6)–M–O(6)*	88.3(2)	88.5(3)	85.1(7)	86.1(4)

Symmetry operation: (*) $-x, y, \frac{1}{2} - z$.

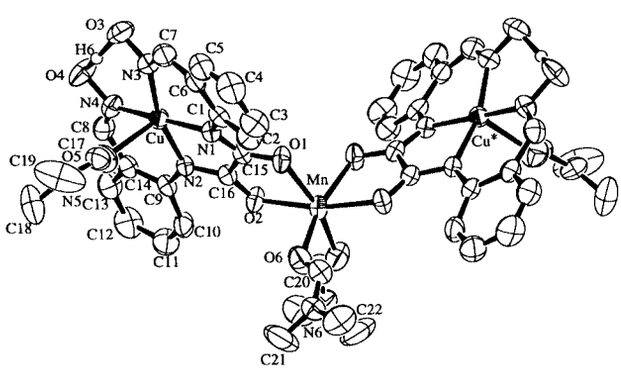

Fig. 2 An ORTEP view of [Mn{Cu(HL)(DMF)}$_2$(DMF)$_2$] **1** with the atom numbering scheme.

on the basal plane and O(5) of DMF at the apex. The Cu–N bond distances range from 1.976(4) to 2.014(4) Å. The axial Cu–O(5) bond distance is 2.378(4) Å which is elongated due to the Jahn–Teller effect of the d^9 electronic configuration. The Cu is displaced by 0.179 Å from the basal least-squares plane toward O(5). One proton of the oxime group is deprotonated to form a N–O–H···O–N hydrogen bond. The N(3)–O(3)–H(6), N(4)–O(4)–H(6) and O(3)–H(6)–O(4) angles are 98.4, 102.0 and 156.9°, respectively. The O(3)···O(4) separation is short (2.381(6) Å), suggesting that the hydrogen bond is very strong. The oxamidatomanganese entity forms a good coplane, but the [Cu(HL)]$^-$ molecule is not coplanar. The least-squares plane defined by Cu, N(1), N(2), N(3) and N(4) and that defined by N(1), N(2), C(15), C(16), O(1), O(2) and Mn are bent at the N(1)···N(2) edge with a dihedral angle of 21.02° (see Fig. 2). The Mn^{II} has a *cis*-octahedral geometry with four oxamidate oxygens, O(1), O(2), O(1)* and O(2)*, and two DMF oxygens, O(6) and O(6)* (* indicates the symmetry operation of $-x, y, \frac{1}{2} - z$). The Mn–O bond distances range from 2.159(4) to 2.174(4) Å. The Cu^{II}···Mn^{II} separation is 5.491(1) Å.

The {Cu(HL)}$^-$ parts in complexes **1**–**4** are essentially similar. Some noticeable differences in the structures are seen in the geometry around the M^{II}. The average M–O bond distance decreases in the order: **1** (2.167) ≈ **2** (2.165) > **4** (2.085) > **3** (2.038 Å). Notably, **1** and **2** have the same M–O bond distance in spite of the markedly differing ionic radius between Mn^{II} (0.97) and Co^{II} (0.89 Å).[29] The M–O bond distance of **2**–**4** decreases with decreasing ionic radius of the M^{II}. The M···Cu intermetallic distances separated by the oxamidate bridge are in a similar order: **1** (5.491(1)) ≈ **2** (5.490(2)) > **4** (5.385(1)) > **3** (5.334(3) Å).

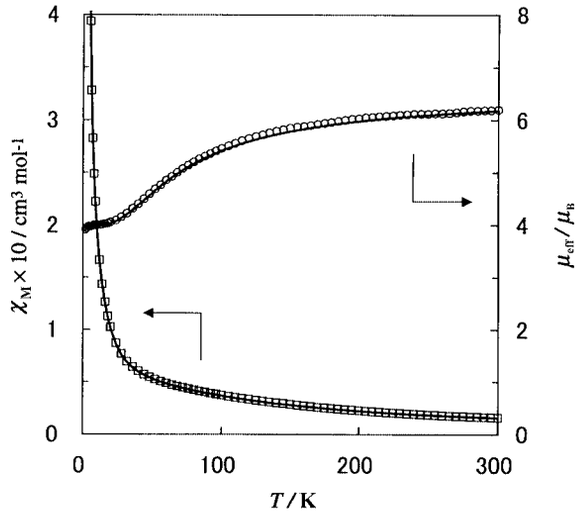

Fig. 3 χ_m *vs.* T and μ_{eff} *vs.* T plots for [Mn{Cu(HL)(DMF)}$_2$(DMF)$_2$] **1**.

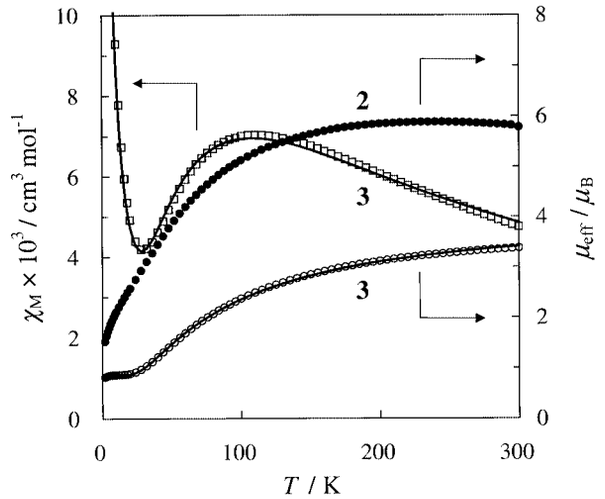

Fig. 4 χ_m *vs.* T plots for [Co{Cu(HL)(DMF)}$_2$(DMF)$_2$] **2** and χ_m *vs.* T and μ_{eff} *vs.* T plots for [Ni{Cu(HL)(DMF)}$_2$(DMF)$_2$] **3**.

Magnetic properties

The room-temperature magnetic moment of complex **1** is 6.20 μ_B (per molecule) that is slightly smaller than the spin-only value (6.40 μ_B) expected for two Cu^{II} ($S = 1/2$) and one Mn^{II} ($S = 5/2$). The effective magnetic moment decreased with decreasing temperature to a near plateau value of 3.90 μ_B below 20 K (Fig. 3). The plateau moment is close to the spin-only value for $S_T = 3/2$ (3.87 μ_B) resulting from the antiferromagnetic spin coupling in the Cu^{II}–Mn^{II}–Cu^{II} system. The interaction between the terminal Cu^{II} can be ignored because complex **4** (CuZnCu) shows little temperature dependence of magnetic moment (1.78 μ_B at 300 K and 1.76 μ_B at 10 K). Based on the spin Hamiltonian $H = -2JS_{Mn}(S_{Cu1} + S_{Cu2})$, the magnetic susceptibility expression for the Cu^{II}–Mn^{II}–Cu^{II} system is given by eqn. (1),[30] where N is Avogadro's number,

$$\chi_m = \{Ng^2\beta^2/4k(T - \theta)\}[84\exp(5J/kT) + 35\exp(-2J/kT) + 10\exp(-7J/kT) + 35]/[4\exp(5J/kT) + 3\exp(-2J/kT) + 2\exp(-7J/kT) + 3] + N_\alpha \quad (1)$$

g the Lande g factor, β the Bohr magneton, k the Boltzmann constant, J the exchange integral, T the absolute temperature, θ the Weiss constant and N_α the temperature-independent paramagnetism. The same g factor is applied for four different spin states, ($S = 7/2$, $S' = 1$), ($S = 5/2$, $S' = 1$), ($S = 3/2$, $S' = 1$) and ($S = 5/2$, $S' = 0$), defined by $S = S_{Mn} + S_{Cu1} + S_{Cu2}$ and $S' = S_{Cu1} + S_{Cu2}$. A good magnetic simulation is obtained by eqn. (1), using the best-fit parameters $J = -14$ cm^{-1}, $g = 2.07$, and $N_\alpha = 120 \times 10^{-6}$ cm^3 mol^{-1} and $\theta = -0.1$ K (see Fig. 3). The discrepancy factor defined as $R(\chi) = [\Sigma(\chi_{obs} - \chi_{calc})^2/\Sigma(\chi_{obs})^2]^{1/2}$ was 2.99×10^{-3}.

Oxamato-bridged $Cu^{II}Mn^{II}Cu^{II}$ complexes with a similar trinuclear core structure are known.[31] It is noted that their exchange integrals (−14.7 to −16.9 cm^{-1}) are comparable to that observed for **1** ($J = -14$ cm^{-1}). Comparable exchange integrals (−11.7 to −18.3 cm^{-1}) have also been reported for other complexes with Cu^{II} and Mn^{II} combined by oxamido or oxamato bridges.[10,32,33]

The μ_{eff} *vs.* T curve of complex **2** is given in Fig. 4. The effective magnetic moment at room temperature is 5.78 μ_B that is larger than the spin-only value (4.24 μ_B) expected for two Cu^{II} ($S = 1/2$) and one Co^{II} ($S = 3/2$). The magnetic moment slightly increased with decreasing temperature to a maximum of 5.88 μ_B near 245 K and then continuously decreased to 1.52 μ_B at 2 K. Such magnetic behavior is probably due to a large orbital contribution arising from the $^4T_{1g}$ ground term of Co^{II}.[34] An antiferromagnetic interaction may operate between the adjacent Cu^{II} and Co^{II}, but the exchange integral could not be evaluated because of the orbital contribution from the Co^{II}.

The μ_{eff} *vs.* T and χ_m *vs.* T curves of complex **3** are shown in Fig. 4. The effective magnetic moment at room temperature is 3.38 μ_B, which is small relative to the spin-only value (3.74 μ_B) expected for two Cu^{II} ($S = 1/2$) and one Ni^{II} ($S = 1$). The magnetic moment decreased with decreasing temperature to 0.82 μ_B at 2 K. The magnetic behavior indicates significant antiferromagnetic interaction between the adjacent Cu^{II} and Ni^{II} through the oxamidate bridge. The magnetic susceptibility expression for the Cu^{II}–Ni^{II}–Cu^{II} system is given by eqn. (2),[30]

$$\chi_m = \{2Ng^2\beta^2/kT\}[5\exp(4J/kT) + 1 + \exp(2J/kT)]/[5\exp(4J/kT) + 3 + \exp(-2J/kT) + 3\exp(2J/kT)] + N_\alpha \quad (2)$$

based on the Heisenberg model $H = -2JS_{Ni}(S_{Cu1} + S_{Cu2})$. Magnetic simulations with this equation gave a poor fitting in the low temperature region below 60 K. A sharp increase in χ_m below 10 K suggests a secondary contribution such as an intermolecular interaction or contamination with a paramagnetic impurity. Thus, magnetic simulations were carried out using the modified expression (2′), where ρ is the fraction

$$\chi_m = (1 - \rho)\{2Ng^2\beta^2/k(T - \theta))\}[5\exp(4J/kT) + 1 + \exp(2J/kT)]/[5\exp(4J/kT) + 3 + \exp(-2J/kT) + 3\exp(2J/kT)] + (2Ng^2\beta^2\rho/3kT) + N_\alpha \quad (2')$$

of paramagnetic impurity. The paramagnetic impurity is presumed to be a nickel(II) species because no copper(II) complex was isolated from H_4L. As seen in Fig. 4, a tolerable magnetic simulation is achieved using $J = -48$ cm^{-1}, $g = 2.06$, $N_\alpha = 400 \times 10^{-6}$ cm^3 mol^{-1}, and $\rho = 0.08$. The discrepancy factor $R(\chi)$ was 6.98×10^{-2}.

Extension to an ordered network

The trinuclear complexes **1**–**4** are expected to combine another metal ion through the dioximate bridge to give a polymeric compound. This is possible only when the trinuclear CuMCu core does not cause metal scrambling in the reaction with a third metal ion. In order to avoid such a problem, in this work **1** (CuMnCu) was treated with Mn^{II}. It is considered that Mn^{II} prefers the dioximate oxygens to the N_4 cavity of L^{4-}.

In our first attempt using LiOH as the base in CH_3CN, complex **1** formed a stable dilithium salt that had little reactivity

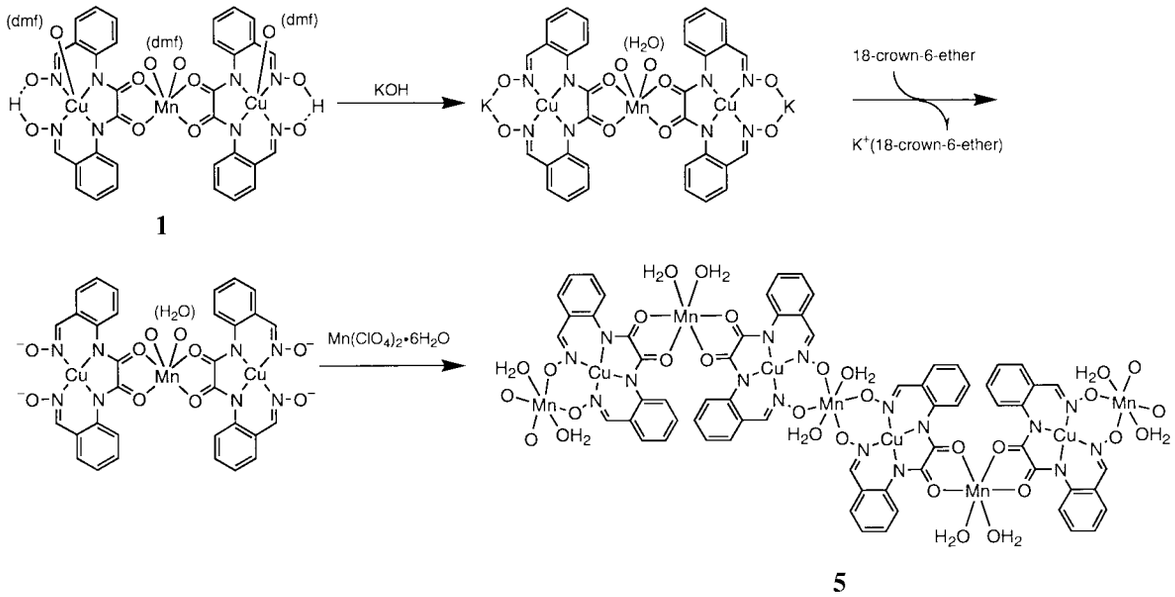

Scheme 1 Synthesis of $Mn\{Cu(L)\}(H_2O)_4$ **5** from complex **1**.

toward Mn^{II}. Thus, KOH was used fully to deprotonate the dioxime proton and 18-crown-6 added to eliminate potassium ion by complexation. To the resulting solution was added manganese(II) perchlorate hexahydrate, precipitating crystalline $Mn\{Cu(L)\}(H_2O)_4$ **5**. The synthesis is shown in Scheme 1.

Compound **5** shows no IR vibration in the region 2300–3000 cm^{-1}, indicating that the dioxime part is fully deprotonated and involved in polymeric structure formation. Another notable feature is the lack of the ν(C=O) vibration of DMF and the appearance of a ν(OH) mode around 3500 cm^{-1}. This means that the DMF molecules in **1** are replaced with water molecules in **5**. In fact, analytical data for **5** indicate the presence of four water molecules instead of DMF. The reflectance spectrum of **5** resembles that of **1** and shows two visible bands at 500 and 590 nm. Together with the crystallographic result for **1**, the most likely structure of **5** is as in Scheme 1.

The cryomagnetic properties of complex **5** were studied in the temperature range 2–300 K. The χ_m *vs.* T and μ_{eff} *vs.* T plots are given in Fig. 5. The effective magnetic moment at room temperature is 5.99 μ_B, which is slightly smaller than the spin-only value (6.16 μ_B) expected for uncoupled Cu^{II} ($S = 1/2$) and Mn^{II} ($S = 5/2$) ions. The magnetic moment decreased with decreasing temperature to a minimum value of 5.04 μ_B near 60 K. This is close to the spin-only value for $S_T = 2$ (4.90 μ_B) arising from antiferromagnetic spin coupling between Cu^{II} ($S = 1/2$) and Mn^{II} ($S = 5/2$). This fact implies a strong antiferromangetic interaction between Cu^{II} and Mn^{II} through the *cis* dioximate bridge in spite of a large intermetallic distance (*ca.* 3.65–3.75 Å[18]). With further decrease in temperature, the magnetic moment of **5** increased to a maximum value of 17.80 μ_B at 5 K and then decreased below this temperature. The cryomagnetic behavior suggests that **5** is a weak ferromagnet exhibiting a weak antiferromagnetic interaction between the ferrimagnetic chains.

The field-cooled magnetization (FCM) under an applied field of 5 G increased rapidly below 9 K to a maximum at 5.2 K, decreased to a minimum at 4.2 K, and then increased to 67 cm^3 G mol^{-1} at 2.0 K (Fig. 6). When the applied field was switched off at 2 K a remnant magnetization of 34 cm^3 G mol^{-1} remained that decreased upon warming and vanished at ≈8 K. The zero-field-cooled magnetization (ZFCM) under an applied field of 5 G showed a maximum at 5.5 K. From these studies the magnetic phase transition temperature (T_C) was determined to be 5.5 K. The ZFCM curve shows another phase transition at 3.6 K, but its origin was not studied.

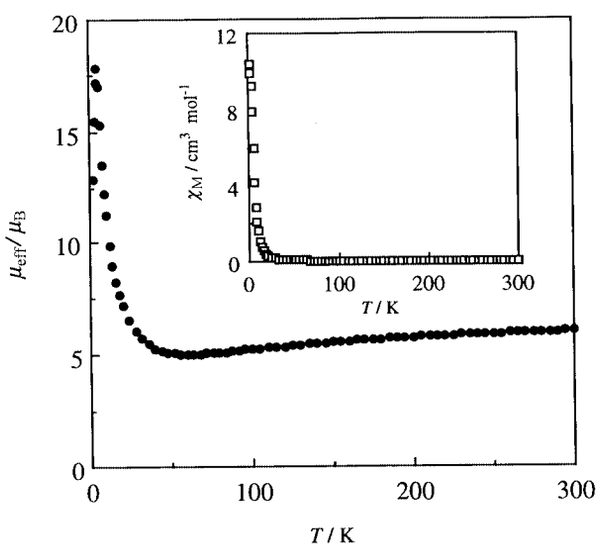

Fig. 5 χ_m *vs.* T and μ_{eff} *vs.* T plots for $Mn\{Cu(L)\}(H_2O)_4$ **5**.

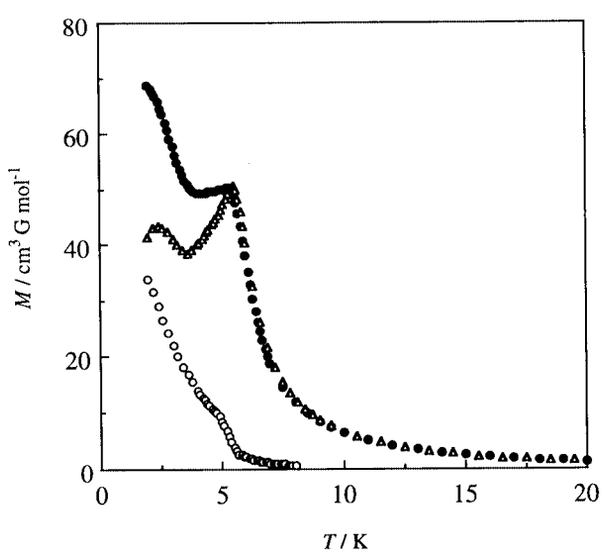

Fig. 6 Field-cooled magnetization (FCM) (●) under 5 G, zero-field-cooled magnetization (ZFCM) (○), and remnant magnetization (RM) (△) for $Mn\{Cu(L)\}(H_2O)_4$ **5**.

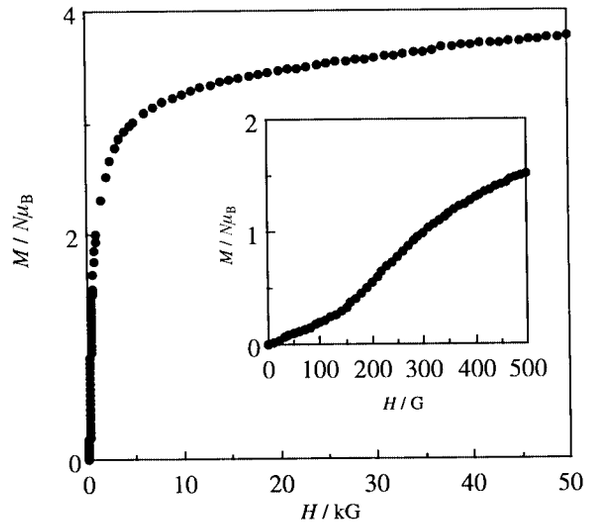

Fig. 7 Field dependences of magnetization for Mn{Cu(L)}$(H_2O)_4$ **5** (determined at 2 K).

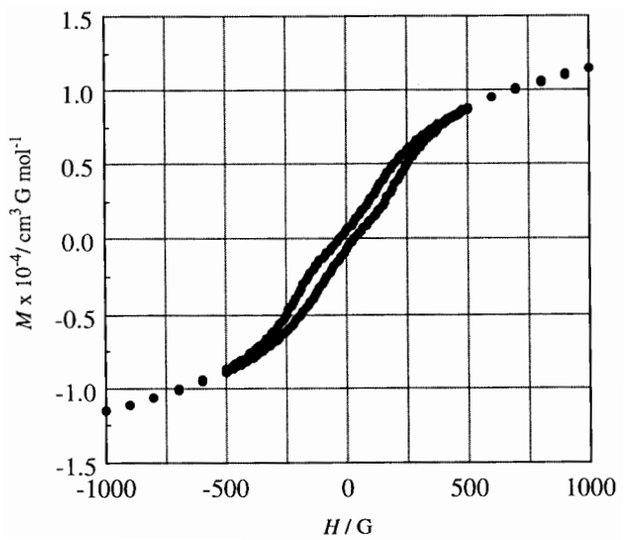

Fig. 8 Hysteresis curve of Mn{Cu(L)}$(H_2O)_4$ **5**.

The field dependences of magnetization measured at 2 K are given in Fig. 7. The magnetization increased sharply with applied field to demonstrate a magnetic ordering in the bulk. The magnetization at 50 kG is 3.78 $N\mu_B$ adding support to antiferromagnetic coupling between the adjacent Cu^{II} ($S = 1/2$) and Mn^{II} ($S = 5/2$). An expansion in the field of 0–500 G is given in the insert where the field-dependence curve shows a break around 150 G. This means a phase transition from a weak ferromagnet to a ferromagnet with applied magnetic field. The hysteresis curve of **5** was determined at 2 K in the applied field of −1000 to +1000 G (see Fig. 8). It shows a remnant magnetization of 672 cm^3 G mol^{-1} and a coercive force of 30 G. The hysteresis curve shows a break due to the phase transition near 150 G.

The magnetic phase transition is further supported by magnetization studies under different magnetic fields (Fig. 9). The *M vs. T* curves at 50, 100 and 200 G show a break around 5 K, whereas the curves at 250 and 300 G show no such a break. Thus, the weak antiferromagnetic interaction between the ferrimagnetic chains is overcome by the weak applied field.

In conclusion the oxamide/dioxime ligand is promising for providing complex-based magnetic materials. This work illustrates a stepwise synthesis of magnetic materials using a 'complex bridge'.

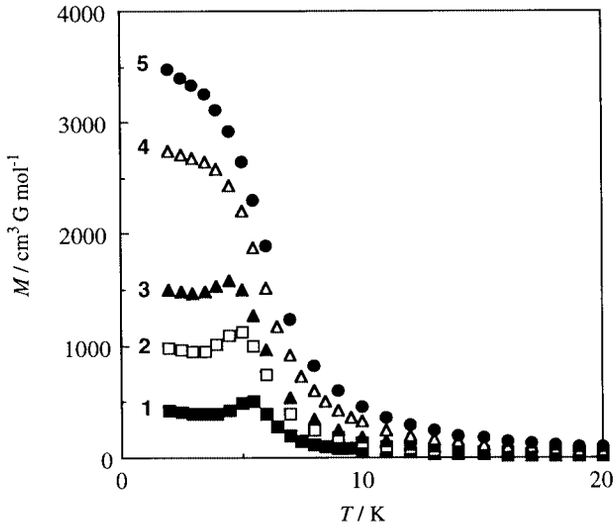

Fig. 9 *M vs. T* curves of Mn{Cu(L)}$(H_2O)_4$ **5** under different applied fields (measured at 2 K): (1) 50, (2) 100, (3) 200, (4) 250, (5) 300 G.

Acknowledgements

This work was supported by Grants-in-Aid for Scientific Research (No. 09440231), Scientific Research on Priority Area 'Metal-assembled Complexes' (No. 10149106) and an International Scientific Research Program (No. 09044093) from the Ministry of Education, Science and Culture, Japan.

References

1 Proceedings of the NATO Advanced Research Workshop on Magnetic Molecular Materials, Kluwer, Dordrecht, 1990.
2 O. Kahn, *Molecular Magnetism*, VCH, Weinhem, 1993; O. Kahn, in *Inorganic Materials*, John Wiley & Sons Inc., New York, 1992, p. 59.
3 O. Kahn, *Adv. Inorg. Chem.*, 1995, **43**, 179.
4 M. M. Turnbull, T. Sugimoto and L. K. Thompson, *ACS Symp. Ser.*, 1996, **644.**
5 H. Tamaki, Z. J. Zhong, N. Matsumoto, S. Kida, M. Kiokawa, N. Achiwa, Y. Hashimoto and H. Ōkawa, *J. Am. Chem. Soc.*, 1992, **114**, 6974; H. Tamaki, M. Mitsumi, K. Nakamura, N. Matsumoto, S. Kida, H. Ōkawa and S. Iijima, *Chem. Lett.*, 1992, 1875; H. Ōkawa, N. Matsumoto, H. Tamaki and M. Ohba, *Mol. Cryst. Liq. Cryst.*, 1993, **233**, 257.
6 H. Ōkawa, M. Mitsumi, M. Ohba, M. Kodera and N. Matsumoto, *Bull. Chem. Soc. Jpn.*, 1994, **67**, 2139.
7 H. Ōkawa, Y. Kawahara, M. Mikuriya and S. Kida, *Bull. Chem. Soc. Jpn.*, 1980, **53**, 549; H. Ōkawa, N. Matsumoto, M. Koikawa, K. Takeda and S. Kida, *J. Chem. Soc., Dalton Trans.*, 1990, 1383; M. Ohba, M. Shiozuka, N. Matsumoto and H. Ōkawa, *Bull. Chem. Soc. Jpn.*, 1992, **65**, 1988.
8 K. Nonoyama, H. Ojima, K. Ohkiand and M. Nonoyama, *Inorg. Chim. Acta*, 1980, **41**, 155.
9 A. Bencini, M. Di Vaira, A. C. Fabretti, D. Gatteschi and C. Zanchini, *Inorg. Chem.*, 1984, **23**, 1620.
10 Y. Pei, O. Kahn, K. Nakatani, E. Codjovi, C. Mathoniere and J. Sletten, *J. Am. Chem. Soc.*, 1991, **113**, 6558.
11 Y. Pei, O. Kahn, J. Sletten, J. P. Renard, R. Georges, J. C. Gianduzzo, J. Curely and Q. Xu, *Inorg. Chem.*, 1988, **27**, 47.
12 Y. Pei, K. Nakatani, O. Kahn, J. Sletten and J. P. Renard, *Inorg. Chem.*, 1989, **28**, 3170.
13 R. Beckett, R. Colton, B. F. Hoskins, R. L. Martin and D. G. Vince, *Aust. J. Chem.*, 1969, **22**, 2527; R. Backett and B. F. Hoskins, *J. Chem. Soc., Dalton Trans.*, 1972, 291.
14 J. A. Bertrand, J. H. Smith and P. Garyeller, *Inorg. Chem.*, 1974, **13**, 1649.
15 Y. Agnus, R. Louis, R. Jesser and R. Weiss, *Inorg. Nucl. Chem. Lett.*, 1976, **12**, 455.
16 A. Chakravorty, *Coord. Chem. Rev.*, 1974, **13**, 1; J. G. Mohanty, S. Baral, R. P. Singh and A. Chakravorty, *Inorg. Nucl. Chem. Lett.*, 1974, **10**, 655; D. Data and N. Chakravorty, *Inorg. Chem.*, 1983, **22**, 1611; S. Baral and A. Chakravorty, *Inorg. Chim. Acta*, 1980, **39**, 1; B. K. Ghosh, R. Mukherjee and A. Chakravorty, *Inorg. Chem.*,

1987, **26**, 1946; P. Basu, S. Pal and A. Chakravorty, *Inorg. Chem.*, 1988, **27**, 1850.
17 G. A. Nicholson, C. R. Lazarus and B. J. McCormick, *Inorg. Chem.*, 1980, **19**, 192; G. A. Nicholson, J. L. Petersen and B. J. McCormick, *Inorg. Chem.*, 1980, **19**, 195.
18 D. Luneau, H. Oshio, H. Ōkawa and S. Kida, *Chem. Lett.*, 1989, 443; H. Ōkawa,M. Koikawa, S. Kida, D. Luneau and H. Oshio, *J. Chem. Soc.*, *Dalton Trans.*, 1990, 469; D. Luneau, H. Oshio, H. Ōkawa, M. Koikawa and S. Kida, *Bull. Chem. Soc. Jpn.*, 1990, **63**, 2212; D. Luneau, H. Oshio, H. Ōkawa and S. Kida, *J. Chem. Soc.*, *Dalton Trans.*, 1990, 2282.
19 Z. J. Zhong, H. Ōkawa, N. Matsumoto, H. Sakiyama and S. Kida, *J. Chem. Soc.*, *Dalton Trans.*, 1991, 497.
20 R. Ruiz, M. Julve, J. Faus, F. Lloret, M. C. Muñoz, Y. Journaux and C. Bois, *Inorg. Chem.*, 1997, **36**, 3434.
21 E. Colacio, J. M. Dominguez-Vera, A. Escuer, R. Kivekäs and A. Romerosa, *Inorg. Chem.*, 1994, **33**, 3914.
22 F. Birkelbach, M. Winter, U. Flörke, H.-J. Haupt, C. Butzlaff, M. Lengen, E. Bill, A. X. Trautwein, K. Wieghardt and P. Chaudhuri, *Inorg. Chem.*, 1994, **33**, 3990; C. Krebs, M. Winter, T. Weyhermuller, E. Bill, K. Wieghardt and P. Chaudhuri, *J. Chem. Soc.*, *Chem. Commun.*, 1995, 1913; C. N. Verani, E. Rentschler, T. Weyhermuller, E. Bill and P. Chaudhuri, *J. Chem. Soc.*, *Dalton Trans.*, 2000, 251.
23 E. A. Boudreaux and L. N. Mulay, *Theory and Applications of Molecular Paramagnetism*, Wiley, New York, 1976, pp. 491–494.
24 W. L. F. Armarego and R. E. Wilette, *J. Chem. Soc.*, 1965, 1258.
25 TEXSAN, Crystal Structure Analysis Package, Molecular Structure Corporation, Houston, TX, 1985 and 1992.
26 R. Blinc and D. Hadzi, *J. Chem. Soc.*, 1958, 4536.
27 K. Burger, I. Ruff and F. Ruff, *J. Inorg. Nucl. Chem.*, 1965, **27**, 179.
28 C. K. Johnson, ORTEP, Report 3794, Oak Ridge National Laboratory, Oak Ridge, TN, 1965.
29 D. E. Shannon and C. T. Prewitt, *Acta Crystallogr.*, *Sect. B*, 1969, **25**, 925; R. D. Shannon, *Acta Crystallogr.*, *Sect. A*, 1976, **32**, 751.
30 E. Sinn and C. M. Harris, *Coord. Chem. Rev.*, 1969, **4**, 391.
31 J.-P. Costes, J.-P. Laurent, J. M. M. Sanchez, J. S. Varela, M. Ahlgren and M. Sundberg, *Inorg. Chem.*, 1997, **36**, 4641.
32 Y. Pei, Y. Journaux and O. Kahn, *Inorg. Chem.*, 1988, **27**, 399; O. Kahn, Y. Pei, M. Verdaguer, J. P. Renard and J. Sletten, *J. Am. Chem. Soc.*, 1988, **110**, 782; K. Nakatani, P. Bergerat, E. Codjovi, C. Mathoniere, Y. Pei and O. Kahn, *Inorg. Chem.*, 1991, **30**, 3977; K. Nakatani, J. Sletten, S. Halut-Desporte, S. Jeannin, Y. Jeannin and O Kahn, *Inorg. Chem.*, 1991, **30**, 164; C. Mathoniere, O. Kahn, J. C. Daran, H. Hilbig and F. H. Koller, *Inorg. Chem.*, 1993, **32**, 4057.
33 L. Mörgenstern-Badarau and H. H. Wickman, *Inorg. Chem.*, 1985, **24**, 1889.
34 F. E. Mabbs and D. J. Machin, *Magnetism and Transition Metal Complexes*, Chapman and Hall, London, 1973.